Available online at www.sciencedirect.com
SCIENCE DIRECT®
Wave Motion 39 (2004) 227–240
WAVE MOTION
www.elsevier.com/locate/wavemoti

Wave propagation in partially saturated porous media: simulation of a second slow wave

José M. Carcione [a,*], Fabio Cavallini [a], Juan E. Santos [b], Claudia L. Ravazzoli [b], Patricia M. Gauzellino [b]

[a] *Istituto Nazionale di Oceanografia e di Geofisica Sperimentale (OGS), Borgo Grotta Gigante 42c, 34010 Sgonico, Trieste, Italy*
[b] *Facultad de Ciencias Astronómicas y Geofísicas, Universidad Nacional de La Plata, Argentina*

Received 20 January 2003; received in revised form 8 September 2003; accepted 7 October 2003

Abstract

We simulate wave propagation in a partially saturated porous medium, where the novel feature is the presence of a second slow wave due to capillary forces. The pores are filled with a wetting fluid and a non-wetting fluid, and the model, based on a Biot-type three-phase theory, predicts three compressional waves and one shear wave. Moreover, the theory models the realistic attenuation levels observed in rocks. Attenuation is modeled with exponential relaxation functions which allow a differential formulation based on memory variables. The wavefield is obtained with a grid method based on the Fourier differential operator and a Runge–Kutta time-integration algorithm. Since the presence of slow quasi-static modes makes the differential equations stiff, a time-splitting integration algorithm is used to solve the stiff part analytically. The modeling is second-order accurate in the time discretization and has spectral accuracy in the calculation of the spatial derivatives. Surface-tension effects in the fluids, which are not considered in the classical Biot theory, cause the presence of a second slow wave, which is faster than the classical Biot slow wave. The present modeling algorithm can be used to study the conditions for which this new wave can be detected in laboratory experiments.

1. Introduction

The acoustics of porous media is an important field of research in seismic exploration [4,6,19]. Regional exploration seismology aimed at the discovery of hydrocarbon reservoirs has been largely based on simplified rheological models. The new exploration scenario is confined to reservoir areas and involves the presence of oil wells, and data from seismic logs and well seismics, which have enough resolution to "see" the effects of bulk properties, porosity, permeability, fluid saturation and fluid–solid interaction on the seismic pulse. The correct description of the reservoir response requires to model reservoir rocks by porous media and use numerical simulation based on the full wave equation.

Biot [3] developed a theory of propagation of elastic waves in porous media, where the two-phase material is considered as a continuum, ignoring the microscopic level. Within this context, the macroscopic variables follow the laws of continuum mechanics. Basically, the theory assumes that anelastic effects arise from viscous interaction

* Corresponding author. Tel.: +39-040-2140345; fax: +39-040-327521.
E-mail address: jcarcione@ogs.trieste.it (J.M. Carcione).

0165-2125/$ – see front matter © 2003 Elsevier B.V. All rights reserved.
doi:10.1016/j.wavemoti.2003.10.001

between the fluid and the solid. Biot demonstrated the existence of two kinds of compressional waves in a porous medium: the fast wave for which the solid and fluid displacements are in phase, and the slow wave for which the displacements are out of phase. At low frequencies, the slow wave becomes diffusive, since viscosity effects dominate (the boundary layer is thick compared to the pore size). At high frequencies, tangential slip occurs (the boundary layer is thin), the inertial effects are predominant and the slow wave is a propagation mode. Plona [23] was the first to observe the second (slow) P wave in water-saturated sintered glass beads. This wave contributes to the attenuation of the fast wave by mode conversion at inhomogeneities.

However, Biot's theory considers a fully saturated medium. i.e., a single fluid. A generalization of Biot's theory to partial saturation is given in [25–27]. When the pore space is filled with two immiscible fluids, capillary forces are important, and the theory predicts a third compressional wave (i.e., a second slow wave). The presence of slow waves constitutes a mechanism of attenuation of the primary (fast) compressional wave by mode conversion. Chin et al. [10] have analyzed Plona's data [23] and are able to assess the attenuation in Plona's experiments. They used a generalized ray expansion algorithm, where multiple reflections and converted modes can be easily identified.

Moreover, it is well known that Biot-type theories do not appropriately model the levels of wave attenuation observed in rocks [20]. Gurevich et al. [14] performed experiments on a sample made of sintered glass beads, and used the Biot's pore form factor as a fitting parameter to model the amplitudes. This factor controls the behavior of the dynamic permeability/tortuosity function. However, although this approach successfully describes the wave propagation properties of synthetic porous media such as sintered glass beads, in natural porous media such as sandstone, discrepancies between Biot theory and measurements are due to complex pore shapes and the presence of clay, which are not present in synthetic media. This complexity gives rise to a variety of relaxation mechanisms that contribute to the attenuation of the different wave modes. Stoll and Bryan [28] show that attenuation is controlled by the anelasticity of the skeleton (friction at grain contacts and interaction with the fluid) and by viscodynamic causes. Thus, we model realistic attenuation levels by generalizing the elastic moduli to time-dependent relaxation functions, implying the introduction of additional differential equations [5].

The poro-viscoelastic differential equations have the form $\dot{\mathbf{w}} = \mathbf{M}\mathbf{w}$, where $\mathbf{w}$ is the wavefield vector and $\mathbf{M}$ the propagation matrix (the dot denotes time differentiation). As in the poroacoustic case [9], all the eigenvalues of $\mathbf{M}$ have negative real part. While the eigenvalues of the fast waves have a small real part, the eigenvalues of the slow waves (in the quasi-static regime) have a large real part. The presence of these quasi-static modes makes the differential equations *stiff* [15]. Thus, seismic and sonic modeling are unstable when using explicit time-integration methods. Carcione and Quiroga-Goode [9], in the poroacoustic case, and Carcione [7] and Carcione and Seriani [8] in the poroelastic case, solved this problem by using a splitting or partition method. The propagation matrix can be partitioned into a stiff part and a non-stiff part as $\mathbf{M} = \mathbf{M}_{\mathrm{r}} + \mathbf{M}_{\mathrm{s}}$, where r indicates the regular matrix, and s the stiff matrix. The stiff part is solved analytically and the non-stiff part is solved with an standard explicit method. Snapshots and time histories are obtained by solving the equations of motion with a direct grid algorithm based on the Fourier pseudospectral method for computing the spatial derivatives [6]. An example of wave propagation in a partially saturated sandstone illustrates the potentialities of the theory and simulation algorithm.

2. Equation of motion

The differential equation of motion for a partially saturated porous medium, including capillary effects, have been obtained by Santos et al. [25–27] from first physical principles. The equations of momentum conservation and constitutive equations are given below.

2.1. Conservation of momentum

We consider a porous rock saturated by two immiscible fluids, and denote with the subscripts (and superscripts) w and n quantities related to the wetting and non-wetting phases, respectively. Let v^{s}, $\bar{v}^{\mathrm{n}}$, and $\bar{v}^{\mathrm{w}}$ denote the

particle-velocity vectors of the solid grains, non-wetting fluid and wetting fluid, respectively, and let τ_{ij} be the total stress. We define the relative particle velocities $v_i^{\rm n} = \phi(\bar{v}_i^{\rm n} - v_i^{\rm s})$ and $v_i^{\rm w} = \phi(\bar{v}_i^{\rm w} - v_i^{\rm s})$. Then, the equations of momentum conservation in two-dimensional space (the (x, z)-plane) can be written as

$$\tau_{ix,x} + \tau_{iz,z} = \rho\dot{v}_i^{\rm s} + \rho_{\rm n}S_{\rm n}\dot{v}_i^{\rm n} + \rho_{\rm w}S_{\rm w}\dot{v}_i^{\rm w}, \qquad \tau_{{\rm n},i} = \rho_{\rm n}S_{\rm n}\dot{v}_i^{\rm s} + g_1\dot{v}_i^{\rm n} + g_3\dot{v}_i^{\rm w} + S_{\rm n}^2\left(\frac{\eta_{\rm n}}{\kappa_{\rm n}}\right)v_i^{\rm n},$$
$$\tau_{{\rm w},i} = \rho_{\rm w}S_{\rm w}\dot{v}_i^{\rm s} + g_3\dot{v}_i^{\rm n} + g_2\dot{v}_i^{\rm w} + S_{\rm w}^2\left(\frac{\eta_{\rm w}}{\kappa_{\rm w}}\right)v_i^{\rm w}, \tag{1}$$

where S, η, ρ, and κ denote saturation ($S_{\rm n} + S_{\rm w} = 1$), viscosity, density and permeability, respectively, $i = 1$ and 3 indicate the spatial variables x and z, and a dot above a variable denotes time differentiation. The stresses $\tau_{\rm n}$ and $\tau_{\rm w}$ are defined in Eq. (5). The density coefficients are

$$\rho = (1-\phi)\rho_{\rm s} + \phi(S_{\rm n}\rho_{\rm n} + S_{\rm w}\rho_{\rm w}), \qquad g_1 = \frac{S_{\rm n}\rho_{\rm n}F_{\rm s}}{\phi}, \qquad g_2 = \frac{S_{\rm w}\rho_{\rm w}F_{\rm s}}{\phi}, \qquad g_3 = 0.1\sqrt{g_1 g_2}, \tag{2}$$

where ρ is the total density, ϕ the effective porosity, and $F_{\rm s}$ a structural factor, which can be estimated as [2],

$$F_{\rm s} = \frac{1}{2}\left(1 + \frac{1}{\phi}\right). \tag{3}$$

The quantities g_1, g_2 and g_3 are mass coupling coefficients, representing the inertial effects associated with dynamic interactions between the three phases. The permeabilities are given by

$$\kappa_{\rm n} = \kappa\left(1 - \frac{1-S_{\rm n}}{1-S_{\rm rn}}\right)^2 \quad \text{and} \quad \kappa_{\rm w} = \kappa\left(\frac{1-S_{\rm n}-S_{\rm rw}}{1-S_{\rm rw}}\right)^2, \tag{4}$$

where κ is the absolute permeability, and $S_{\rm rn}$ and $S_{\rm rw}$ are residual saturations. These relations are based on laboratory experiments performed on various porous rocks during imbibition and drainage processes (neglecting hysteresis effects).

2.2. Stress–strain relations

We define $\dot{\xi}_{\rm n} = -\nabla\cdot v^{\rm n}$ and $\dot{\xi}_{\rm w} = -\nabla\cdot v^{\rm w}$, where ξ is the variation of fluid content. Let $p_{\rm n}$ and $p_{\rm w}$ denote the infinitesimal changes of the wetting and non-wetting pressures with respect to the absolute pressures $\bar{p}_{\rm n}$ and $\bar{p}_{\rm w}$, respectively, let ϵ_{ij} denote the strain components of the solid grains, and let $\vartheta = \epsilon_{11} + \epsilon_{33}$ denote the dilatation field. Then, the stress–strain relation have the form

$$\tau_{xx} = K_{\rm c}\vartheta + N(\epsilon_{xx} - \epsilon_{zz}) - B_1\xi_{\rm n} - B_2\xi_{\rm w}, \qquad \tau_{zz} = K_{\rm c}\vartheta - N(\epsilon_{xx} - \epsilon_{zz}) - B_1\xi_{\rm n} - B_2\xi_{\rm w},$$
$$\tau_{xz} = 2N\epsilon_{xz}, \qquad \tau_{\rm n} = -(S_{\rm n} + \beta + \zeta)p_{\rm n} + (\beta+\zeta)p_{\rm w} = B_1\vartheta - M_1\xi_{\rm n} - M_3\xi_{\rm w},$$
$$\tau_{\rm w} = -(S_{\rm w} + \zeta)p_{\rm w} + \zeta p_{\rm n} = B_2\vartheta - M_3\xi_{\rm n} - M_2\xi_{\rm w}, \tag{5}$$

where N is the dry-rock shear modulus, $K_{\rm c}$ the undrained (closed) bulk modulus (in 2D space, $K_{\rm c} = \lambda_{\rm c} + N$, while in 3D space, $K_{\rm c} = \lambda_{\rm c} + 2N/3$, where $\lambda_{\rm c}$ is an undrained Lamé constant). It is

$$K_{\rm c} = \frac{K_{\rm s}(K_{\rm m} + G)}{K_{\rm s} + G}, \tag{6}$$

where K denotes bulk modulus, $K_{\rm m}$ the dry-rock bulk modulus,

$$G = \frac{K_{\rm f}(K_{\rm m} - K_{\rm s})}{\phi(K_{\rm f} - K_{\rm s})}, \tag{7}$$

$$K_{\rm f} = \alpha \left(\frac{\gamma S_{\rm n}}{K_{\rm n}} + \frac{S_{\rm w}}{K_{\rm w}} \right)^{-1}, \tag{8}$$

$$\alpha = 1 + (S_{\rm n} + \beta)(\gamma - 1), \tag{9}$$

$$B_1 = \theta K_{\rm c}[(S_{\rm n} + \beta)\gamma - \beta + (\gamma - 1)\zeta], \qquad B_2 = \theta K_{\rm c}[(S_{\rm w} + (1 - \gamma)\zeta], \tag{10}$$

$$\theta = \left[\delta + \phi \left(\frac{1}{K_{\rm m}} - \frac{1}{K_{\rm c}} \right) \right] \left\{ \alpha \left[\delta + \phi \left(\frac{1}{K_{\rm m}} - \frac{1}{K_{\rm f}} \right) \right] \right\}^{-1}, \tag{11}$$

$$M_1 = -M_3 - \frac{B_1}{\delta K_{\rm m}}, \qquad M_2 = \frac{rB_2}{q} + \frac{\zeta}{q}, \qquad M_3 = -B_2 \left[\frac{r}{q} + \frac{1}{K_{\rm m}\delta} \right] - \frac{\zeta}{q}, \tag{12}$$

$$\beta = \frac{p_{\rm ca}}{p'_{\rm ca}}, \qquad \zeta = \frac{\bar{p}_{\rm w}}{p'_{\rm ca}}, \tag{13}$$

where $p_{\rm ca}$ is the capillary pressure (i.e., the difference between the non-wetting and wetting absolute pressures), and $p'_{\rm ca}$ its derivative with respect to $S_{\rm n}$,

$$\delta = \frac{1}{K_{\rm s}} - \frac{1}{K_{\rm m}}, \tag{14}$$

$$\gamma = \left(1 + \frac{p'_{\rm ca} S_{\rm n} S_{\rm w}}{K_{\rm w}} \right) \left(1 + \frac{p'_{\rm ca} S_{\rm n} S_{\rm w}}{K_{\rm n}} \right)^{-1}, \tag{15}$$

$$r = \frac{S_{\rm n} + \beta}{K_{\rm s}} + \frac{1}{K_{\rm c} - K_{\rm m}} \left[qB_2 + (S_{\rm n} + \beta) \left(1 - \frac{K_{\rm c}}{K_{\rm s}} \right) \right], \tag{16}$$

$$q = \phi \left(\frac{1}{K_{\rm n}} + \frac{1}{p'_{\rm ca} S_{\rm n} S_{\rm w}} \right). \tag{17}$$

The capillary pressure is obtained with the following relation:

$$p_{\rm ca} = A \left[(S_{\rm n} + S_{\rm rw} - 1)^{-2} - \left(\frac{S_{\rm rn}}{S_{\rm n}} \right)^2 (1 - S_{\rm rn} - S_{\rm rw})^{-2} \right]. \tag{18}$$

Having introduced the momentum-conservation and stress–strain equations, we proceed in the next section to recast these equations in the velocity-stress formulation and incorporate viscoelastic dissipation.

3. Velocity-stress formulation

The velocity-stress formulation are first-order (in the space and time variables) differential equations, where the unknown variables are the particle velocities and stress components. The equations of momentum conservation (1) can be rewritten as

$$\begin{aligned} \dot{v}_i^{\rm s} &= \gamma_{11} \Pi_i^{\rm s} + \gamma_{12} \Pi_i^{\rm n} + \gamma_{13} \Pi_i^{\rm w}, \qquad \dot{v}_i^{\rm n} = \gamma_{12} \Pi_i^{\rm s} + \gamma_{22} \Pi_i^{\rm n} + \gamma_{23} \Pi_i^{\rm w}, \\ \dot{v}_i^{\rm w} &= \gamma_{13} \Pi_i^{\rm s} + \gamma_{23} \Pi_i^{\rm n} + \gamma_{33} \Pi_i^{\rm w}, \end{aligned} \tag{19}$$

where

$$\Pi_i^{\rm s} = \tau_{ix,x} + \tau_{iz,z}, \qquad \Pi_i^{\rm n} = \tau_{{\rm n},i} - S_{\rm n}^2 \left(\frac{\eta_{\rm n}}{\kappa_{\rm n}} \right) v_i^{\rm n}, \qquad \Pi_i^{\rm w} = \tau_{{\rm w},i} - S_{\rm w}^2 \left(\frac{\eta_{\rm w}}{\kappa_{\rm w}} \right) v_i^{\rm w}, \tag{20}$$

are the rate of generalized momenta, and $\gamma_{\rm nm}$ are the components of the following symmetric matrix:

$$\mathbf{D}^{-1} = \begin{pmatrix} \rho & \rho_{\rm n} S_{\rm n} & \rho_{\rm w} S_{\rm w} \\ \rho_{\rm n} S_{\rm n} & g_1 & g_3 \\ \rho_{\rm w} S_{\rm w} & g_3 & g_2 \end{pmatrix}^{-1} . \tag{21}$$

The equations corresponding to the stress components are obtained by differentiating equations (5) with respect to the time variable, and noting that the rate of the strain components is [22]

$$\dot{\epsilon}_{ij} = \tfrac{1}{2}(v_{i,j} + v_{j,i}).$$

3.1. Extension to the poro-viscoelastic case

Wave velocities are generally expected to be lower at low frequencies, typical of seismic measurements, than at high frequencies, typical of laboratory experiments. Since the magnitude of this effect cannot be entirely described by Biot-type theories [6,20], additional relaxation mechanisms are required to model the velocity dispersion. Measurements of dry-rock velocities contain all the information about pore shapes and pore interactions, and their influence on wave propagation. Low-frequency wet-rock velocities can be calculated by using Gassmann's equation, i.e., the low-frequency limit of the dispersion relation [12]. High-frequency wet-rock velocities are then given by the unrelaxed velocities. Since dry-rock velocities are practically frequency-independent, the data can be obtained from laboratory measurements.

Viscoelasticity is introduced into the poroelastic equations for modeling a variety of dissipation mechanisms. One of these mechanisms is the squirt-flow [3,21], by which a force applied to the area of contact between two grains produces a displacement of the surrounding fluid in and out of this area. Since the fluid is viscous, the motion is not instantaneous and energy dissipation occurs.

We generalize the effective moduli of the rock $K_{\rm c}$ and N, to time-dependent relaxation functions, and assume that the other coefficients in the potential energy are frequency-independent. The following terms in Eq. (5) are considered: $K_{\rm c}\vartheta$, $N\epsilon_{xx}$, $N\epsilon_{zz}$ and $N\epsilon_{xz}$. Denoting, in general, those terms by $M\epsilon$, this is replaced by $\psi * \epsilon_{,t}$ in the viscoelastic case, where

$$\psi(t) = M\left(1 + \frac{1}{L}\sum_{l=1}^{L}\varphi_l\right)^{-1}\left[1 + \frac{1}{L}\sum_{l=1}^{L}\varphi_l \exp\left(-\frac{t}{\tau_{\sigma l}}\right)\right] H(t), \tag{22}$$

$H(t)$ is the Heaviside function,

$$\varphi_l = \frac{\tau_{\epsilon l}}{\tau_{\sigma l}} - 1 \tag{23}$$

and $\tau_{\epsilon l}$ and $\tau_{\sigma l}$ are sets of relaxation times. Eq. (22) corresponds to a parallel connection of standard linear solid elements. For high frequencies ($t = 0^+$) $\psi = M$.

As in the single-phase viscoelastic case [5], we introduce memory variables in order to avoid the time convolutions. This approach implies the following substitution:

$$M\epsilon \to M\epsilon + \sum_{l=1}^{L} e_l,$$

where e_l, $l = 1, \ldots, L$ are the memory variables, satisfying

$$e_{l,t} = -\frac{1}{\tau_{\sigma l}}\left[M\left(L + \sum_{m=1}^{L}\varphi_m\right)^{-1}\varphi_l\epsilon + e_l\right]. \tag{24}$$

In particular, if one mechanism is considered, Eqs. (5) become

$$\tau_{xx} = K_c\vartheta + N(\epsilon_{xx} - \epsilon_{zz}) - B_1\xi_n - B_2\xi_w + e_1 + e_2,$$
$$\tau_{zz} = K_c\vartheta - N(\epsilon_{xx} - \epsilon_{zz}) - B_1\xi_n - B_2\xi_w + e_1 - e_2, \qquad \tau_{xz} = 2N\epsilon_{xz} + e_3, \tag{25}$$

and

$$e_{1,t} = -\frac{1}{\tau_{\sigma 1}}\left[K_c\left(1 - \frac{\tau_{\sigma 1}}{\tau_{\epsilon 1}}\right)\dot{\vartheta} + e_1\right], \tag{26}$$

$$e_{2,t} = -\frac{1}{\tau_{\sigma 2}}\left[N\left(1 - \frac{\tau_{\sigma 2}}{\tau_{\epsilon 2}}\right)(\dot{\epsilon}_{xx} - \dot{\epsilon}_{zz}) + e_2\right], \tag{27}$$

$$e_{3,t} = -\frac{1}{\tau_{\sigma 2}}\left[N\left(1 - \frac{\tau_{\sigma 2}}{\tau_{\epsilon 2}}\right)(\dot{\epsilon}_{xy} + \dot{\epsilon}_{xz}) + e_3\right], \tag{28}$$

are the memory-variable equations.

The calculation of the phase velocity and attenuation factor requires a Fourier transformation of the constitutive equations to the frequency domain, implying the following substitution:

$$M \to \bar{M},$$

where

$$\bar{M} = M\left(L + \sum_{l=1}^{L}\varphi_l\right)^{-1}\sum_{l=1}^{L}\frac{1 + i\omega\tau_{\epsilon l}}{1 + i\omega\tau_{\sigma l}} \tag{29}$$

with ω the angular frequency. The relaxation times can be expressed in terms of a Q-factor Q_l and a reference frequency f_l as

$$\tau_{\epsilon l} = \frac{1}{2\pi f_l Q_l}\left[\sqrt{Q_l^2 + 1} + 1\right] \tag{30}$$

and

$$\tau_{\sigma l} = \frac{1}{2\pi f_l Q_l}\left[\sqrt{Q_l^2 + 1} - 1\right]. \tag{31}$$

4. Numerical algorithm

The velocity-stress differential equations can be written in matrix form as

$$\dot{\mathbf{w}} = \mathbf{M}\mathbf{w} + \mathbf{s}, \tag{32}$$

where

$$\mathbf{w} = [v_x^s, v_x^n, v_x^w, v_z^s, v_z^n, v_z^w, \tau_{xx}, \tau_{zz}, \tau_{xz}, \tau_n, \tau_w, \{e\}]^T \tag{33}$$

is the velocity-stress vector, $\{e\}$ represents the set of memory variables,

$$\mathbf{s} = [0, 0, 0, 0, 0, 0, s_{xx}, s_{zz}, s_{xz}, s^n, s^w, \{0\}]^T \tag{34}$$

is the source vector, and $\mathbf{M}$ is the propagation matrix containing the spatial derivatives and material properties.

The solution to Eq. (32) subject to the initial condition $\mathbf{w}(0) = \mathbf{w}_0$ is formally given by

$$\mathbf{w}(t) = \exp(t\mathbf{M})\mathbf{w}_0 + \int_0^t \exp(\tau\mathbf{M})\mathbf{s}(t-\tau)\,\mathrm{d}\tau, \tag{35}$$

where $\exp(t\mathbf{M})$ is called evolution operator.

As in the poroacoustic case [9], the eigenvalues of $\mathbf{M}$ have negative real parts and differ greatly in magnitude due to the viscosity terms. The presence of large eigenvalues, together with small eigenvalues, indicates that the problem is stiff. The differential equations are solved with the splitting algorithm introduced by Carcione and Quiroga-Goode [9] for two-phase poroacoustic media, and Carcione [7] for two-phase poroelastic media, and generalized here for three-phase porous media. The propagation matrix can be partitioned as

$$\mathbf{M} = \mathbf{M}_\mathrm{r} + \mathbf{M}_\mathrm{s}, \tag{36}$$

where subscript r indicates the regular matrix, and subscript s the stiff matrix. Let us discretize the time variable as $t = n\,\mathrm{d}t$, where $\mathrm{d}t$ is the time step. The evolution operator can be expressed as $\exp(\mathbf{M}_\mathrm{r} + \mathbf{M}_\mathrm{s})t$. It is easy to show that the product formula

$$\exp(\mathbf{M}\,\mathrm{d}t) = \exp(\tfrac{1}{2}\mathbf{M}_\mathrm{s}\,\mathrm{d}t)\exp(\mathbf{M}_\mathrm{r}\,\mathrm{d}t)\exp(\tfrac{1}{2}\mathbf{M}_\mathrm{s}\,\mathrm{d}t) \tag{37}$$

is second-order accurate in $\mathrm{d}t$ (see [13,30]). Eq. (37) allow us to solve the stiff part separately. Using the Kronecker product "$\otimes$" of two matrices yields

$$\mathbf{M}_\mathrm{s} = \begin{pmatrix} \mathbf{I}\otimes\mathbf{S} & \mathbf{0} \\ \mathbf{0} & \mathbf{0} \end{pmatrix}, \tag{38}$$

where $\mathbf{I}$ is the 2×2 identity matrix. We should solve

$$\dot{\mathbf{v}}_i = \mathbf{S}\mathbf{v}_i \tag{39}$$

for each Cartesian component i, where

$$\mathbf{v}_i = [v_i^\mathrm{s}, v_i^\mathrm{n}, v_i^\mathrm{w}]^\mathrm{T}, \tag{40}$$

and the components of $\mathbf{S}$ are

$$\begin{aligned} &s_{11} = 0, \quad s_{12} = -\gamma_{12}b_\mathrm{n}, \quad s_{13} = -\gamma_{13}b_\mathrm{w}, \quad s_{21} = 0, \\ &s_{22} = -\gamma_{22}b_\mathrm{n}, \quad s_{23} = -\gamma_{23}b_\mathrm{w}, \quad s_{31} = 0, \quad s_{32} = -\gamma_{32}b_\mathrm{n}, \quad s_{33} = -\gamma_{33}b_\mathrm{w}, \end{aligned} \tag{41}$$

where $b_\mathrm{n} = S_\mathrm{n}^2\eta_\mathrm{n}/\kappa_\mathrm{n}$ and $b_\mathrm{w} = S_\mathrm{w}^2\eta_\mathrm{w}/\kappa_\mathrm{w}$.

The solution of the vector differential equation (39) is given by

$$v_i^\mathrm{s}(t) = \mathbf{s}^\mathrm{T}\mathbf{A}^{-1}(\mathrm{e}^{t\mathbf{A}} - \mathbf{I})\begin{pmatrix} v_i^\mathrm{n}(0) \\ v_i^\mathrm{w}(0) \end{pmatrix}, \tag{42}$$

$$\begin{pmatrix} v_i^\mathrm{n}(t) \\ v_i^\mathrm{w}(t) \end{pmatrix} = \mathrm{e}^{t\mathbf{A}}\begin{pmatrix} v_i^\mathrm{n}(0) \\ v_i^\mathrm{w}(0) \end{pmatrix}, \tag{43}$$

where

$$\mathbf{s} = (s_{12}, s_{13})^\mathrm{T}, \qquad \mathbf{A} = \begin{pmatrix} s_{22} & s_{23} \\ s_{32} & s_{33} \end{pmatrix}, \tag{44}$$

and, by Sylvester's formula [24],

$$\mathrm{e}^{t\mathbf{A}} = \frac{1}{\lambda_1 - \lambda_2}[(\lambda_1\,\mathrm{e}^{\lambda_2 t} - \lambda_2\,\mathrm{e}^{\lambda_1 t})\mathbf{I} + (\mathrm{e}^{\lambda_1 t} - \mathrm{e}^{\lambda_2 t})\mathbf{A}] \tag{45}$$

assuming $\lambda_1 \neq \lambda_2$, with λ_1 and λ_2 eigenvalues of $\mathbf{A}$.

The regular operator $\exp(\mathbf{M}_r\,\mathrm{d}t)$ is approximated with a fourth-order Runge–Kutta solver [7]. The output vector is

$$\mathbf{w}^{n+1} = \mathbf{w}^* + \tfrac{1}{6}(\mathrm{d}t)(\Delta_1 + 2\Delta_2 + 2\Delta_3 + \Delta_4), \tag{46}$$

where

$$\Delta_1 = \mathbf{M}_r\mathbf{w}^* + \mathbf{s}^n, \qquad \Delta_2 = \mathbf{M}_r(\mathbf{w}^* + \tfrac{1}{2}(\mathrm{d}t)\Delta_1) + \mathbf{s}^{n+1/2}, \qquad \Delta_3 = \mathbf{M}_r(\mathbf{w}^* + \tfrac{1}{2}(\mathrm{d}t)\Delta_2) + \mathbf{s}^{n+1/2},$$
$$\Delta_4 = \mathbf{M}_r(\mathbf{w}^* + \mathrm{d}t\Delta_3) + \mathbf{s}^{n+1},$$

and $\mathbf{w}^*$ is the intermediate output vector obtained after the operation with the stiff evolution operator.

Note that two operations with (37) imply

$$\exp(2\mathbf{M}\,\mathrm{d}t) = \exp(\tfrac{1}{2}\mathbf{M}_s\,\mathrm{d}t)\exp(\mathbf{M}_r\,\mathrm{d}t)\exp(\mathbf{M}_s\,\mathrm{d}t)\exp(\mathbf{M}_r\,\mathrm{d}t)\exp(\tfrac{1}{2}\mathbf{M}_s\,\mathrm{d}t). \tag{47}$$

Then, $n-1$ stiff operations can be saved in n time steps, if only snapshots of the wavefield at $n\,\mathrm{d}t$ are to be computed. Moreover, $n(1-1/m)$ stiff operations can be saved when computing seismograms with a sampling rate of m time steps.

The resulting algorithm is second-order accurate in time and has spectral accuracy in the space variable. Use of a fourth-order Runge–Kutta algorithm for the non-stiff part allows us to save computer time by using a larger time step compared to lower order methods. The spatial derivatives are calculated with the Fourier method by using the FFT [6,11]. This approximation is "infinitely" accurate for band-limited periodic functions with cutoff spatial wavenumbers which are smaller than the cutoff wavenumbers of the mesh. If the source spectrum is negligible beyond the Nyquist wavenumber, we can consider that there is no significant numerical dispersion due to the spatial discretization.

The periodicity of the Fourier differential operator causes wraparound of the wavefield. In terms of wave propagation, this means that a wave impinging on the left boundary of the grid will return from the right boundary (the numerical artifact called wraparound). In order to eliminate wraparound, an absorbing strip can be implemented at the boundaries of the mesh. This is achieved by replacing in Eq. (32) the operator $\mathbf{M}$ with $\mathbf{M}+\mathbf{\Gamma}$, where $\mathbf{\Gamma}$ is a diagonal matrix whose entries are the damping coefficients defined by exponential functions in the spatial variables [18]. Matrix $\mathbf{\Gamma}$ is zero everywhere except in a narrow band adjacent to the boundary where it is negative. The

Table 1
Material properties for Nivelsteiner sandstone

Grain	Bulk modulus, K_s (GPa)	36
	Density, ρ_s (kg/m^3)	2650
Matrix	Bulk modulus, K_m (GPa)	6.21
	Shear modulus, N (GPa)	4.55
	Porosity, ϕ	0.33
	Permeability, κ (D)	5
	Bulk loss, $Q(K_c)$	30
	Shear loss, $Q(N)$	20
	Reference frequency, f (kHz)	400
Gas	Bulk modulus, K_n (GPa)	0.022
	Density, ρ_n (kg/m^3)	100
	Viscosity, η_n (cP)	0.015
Water	Bulk modulus, K_w (GPa)	2.223
	Density, ρ_w (kg/m^3)	1000
	Viscosity, η_w (cP)	1

solution to this equation is a wave traveling without dispersion, but whose amplitude decreases with distance at a frequency-independent rate. A traveling pulse will, thus, diminish in amplitude without a change of shape.

5. Examples

We consider wave propagation in Nivelsteiner sandstone [1,17]. It is a Miocene quartz sand with very low clay content and has an average grain distribution of 100–300 μm. The material properties of Nivelsteiner sandstone are

Table 2
Phase velocities and attenuation factors at 400 kHz

Wave	Poro-elastic		Poro-viscoelastic	
	v_p (m/s)	α (db/neper/km)	v_p (m/s)	α (db/neper/km)
P1	2550.72	0.0262939/474.72	2498.59	1.16372/21448.5
P2	282.98	$0.881056/0.143382 \times 10^6$	282.89	$0.896390/0.145920 \times 10^6$
P3	427.05	$1.46909/0.158420 \times 10^6$	426.98	$1.48060/0.159688 \times 10^6$
S	1536.04	0.0305172/914.931	1498.62	$1.39406/0.428387 \times 10^5$

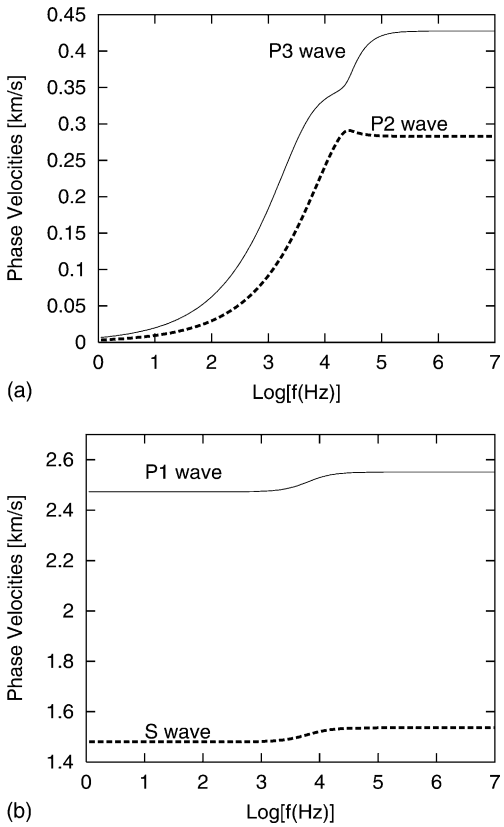

Fig. 1. Phase velocities of the four wave modes propagating in partially saturated Nivelsteiner sandstone versus frequency. Water saturation is 90%. The compressional waves are labeled P1–P3, and the shear wave is labeled S.

given in Table 1. For simplicity, we have assumed that the grains are made of pure quartz. In addition, $S_w = 0.9$, $S_{rn} = S_{rw} = 0.05$, $A = 3$ kPa, and the absolute pressure of the wetting phase is $p_w = 30$ MPa (equivalent to a rock buried at approximately 3 km depth). We have obtained the matrix properties by fitting the experimental data provided by Kelder and Smeulders [17], and assumed that the level of dissipation is that predicted by Biot's theory [1]. The properties of the saturated rock at 400 kHz are given in Table 2.

In the first example we assume no losses due to viscoelastic effects. We consider a 357×357 mesh, with square cells and a grid spacing of 0.175 mm in the ultrasonic range and 14 m in the seismic range. The source has a dominant frequency of 400 kHz and 12.5 Hz, respectively. It is a bulk source ($S_{xx} = S_{zz} = S_{xz} = S_n = S_w$). Fig. 1 shows the phase velocities of the four wave modes versus frequency (Appendix A), where the compressional waves are labeled P1–P3 (inner wavefront), and the shear wave is labeled S. The slow waves have a quasi-static character at low frequencies and become overdamped due to the fluid viscosity. This phenomenon precludes the observation of the slow waves at seismic frequencies.

Snapshots of the wavefield, in the three different phases, are shown in Figs. 2 and 3, for the ultrasonic and seismic ranges. (The time steps, dt, are 12.5 ns and 1 ms, respectively.) As can be appreciated, the snapshots are in agreement

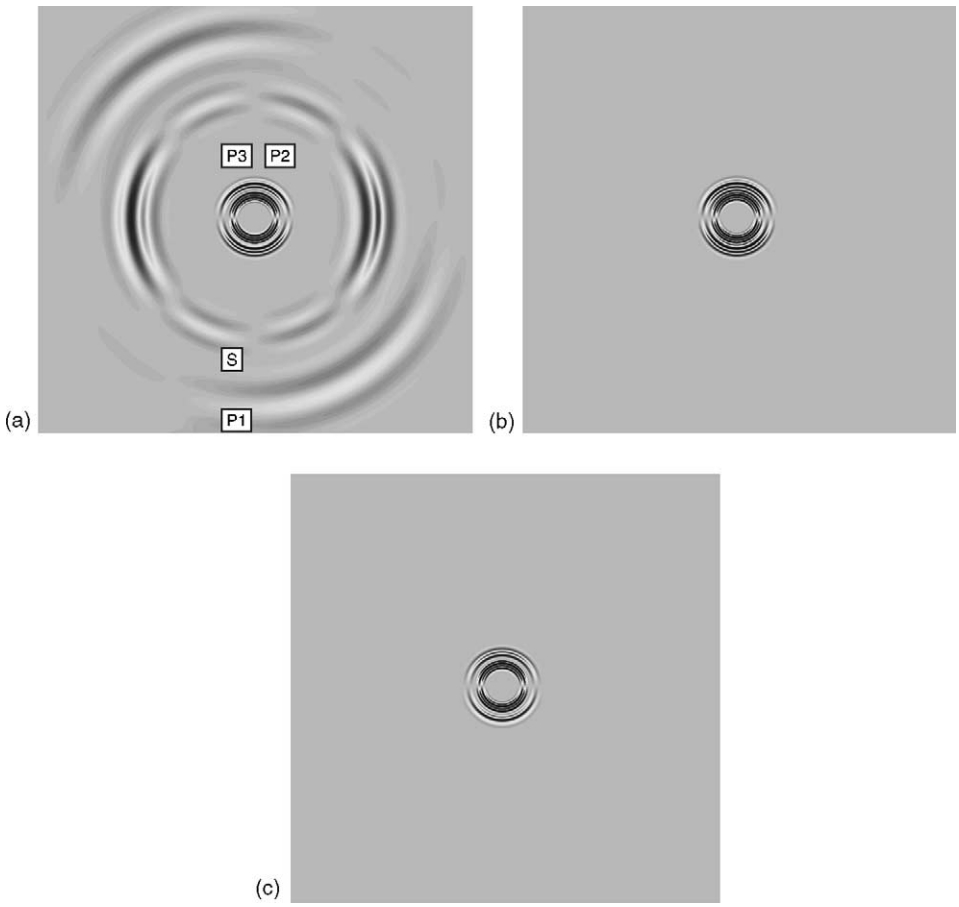

Fig. 2. Snapshots of the particle velocity at 15 μs in the ultrasonic frequency range, corresponding to the rock frame (a), gas phase (b) and water phase (c). The mesh has 357×357 grid points and the grid spacing is 0.175 mm. The compressional waves are labeled P1–P3, and the shear wave is labeled S. The relative amplitudes between the snapshots in (a), (b) and (c) is 1, 224 and 31, respectively, indicating that the slow modes are much stronger in the fluid phases. The label P2 indicates the classical Biot slow wave (solid and fluid motions in opposite phase), and P3 is the new slow wave, due to capillary forces (solid and wetting-fluid motions in opposite phase).

with the predictions of the theory. P1 and S are the usual body waves which we observe in acoustics of material media. They correspond to all the phases moving in phase, and propagate irrespective of the value of the frequency, viscosity, permeabilities.

The numerical experiments show that the motion of the solid for the P2 wave is opposite to those of the fluids, which are in phase. For this reason, we identify this mode with the classical Biot slow wave. With regard to the faster of the two slow compressional waves, referred to as P3 wave, the solid moves in phase with the non-wetting fluid and in opposite phase with the wetting fluid, i.e., the two fluids are in opposite phase. This is a new mode, which is absent in fully saturated porous media.

The slow waves are quasi-static in the seismic range. They can be seen in the fluid phases (Fig. 3b and c) as static modes at the center of the mesh. From the relative amplitudes between the snapshots, we deduce that the wave propagation (in terms of energy) occurs in the solid phase.

In the last example we assume that the rock is viscoelastic, with one relaxation mechanism ($L = 1$) corresponding to each effective modulus, K_c and N. The Q-factor parameters in Eqs. (30) and (31) are $Q(K_c) = 30$ and $Q(N) = 20$, and the reference frequencies are $f(K_c) = f(N) = 400$ kHz. The values of the quality factors given in Table 1 are of the same order of magnitude of those given by Winkler and Nur [31] for partially saturated Massilon sandstone.

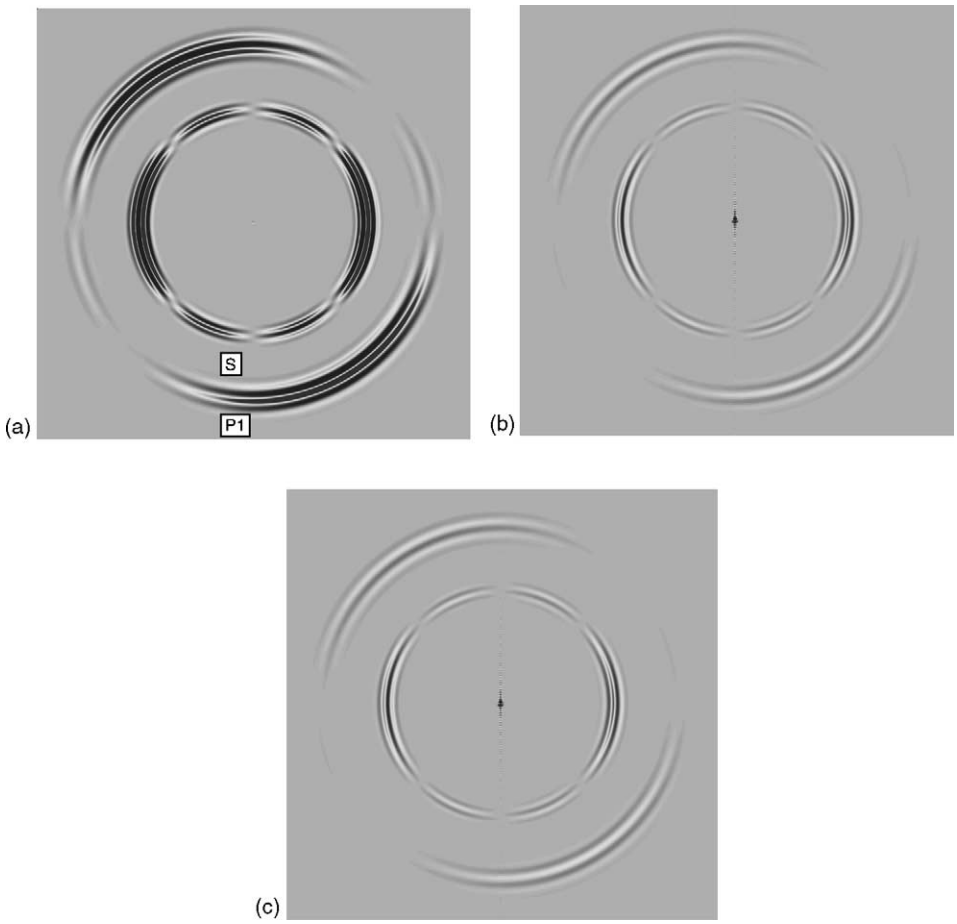

Fig. 3. Snapshots of the particle velocity at 1 s in the seismic frequency range, corresponding to the rock frame (a), gas phase (b) and water phase (c). Water saturation is 90%. The mesh has 357×357 grid points and the grid spacing is 14 m. The labels P1 and S denote the fast compressional and shear waves, and the relative amplitudes indicate that the energy is mainly in the solid phase.

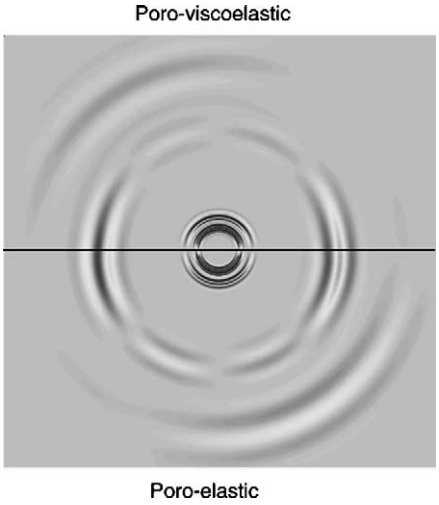

Fig. 4. Snapshot of the rock-frame vertical particle velocity at 15 μs, where the upper half-space is poro-viscoelastic and the lower half-space is poro-elastic. Water saturation is 90%.

Tao et al. [29] and Jones et al. [16] also report quality factor values of the same order for rocks. Finally, Arntsen and Carcione [1] have used shear and dilatational quality factor equal to 10 to fit micro-seismograms from laboratory experiments, at the same frequency indicated in Table 1. Table 2 compares the values of the phase velocities and attenuation factors for the poro-elastic and poro-viscoelastic cases. Rock viscoelasticity affects mainly the waves of the first kind. Fig. 4 shows a snapshot of the rock-frame vertical particle velocity at 15 μs, where the upper half-space is poro-viscoelastic and the lower half-space is poro-elastic. The attenuation of the P1 and S waves in the upper-half-space is evident.

6. Conclusions

We have developed a numerical algorithm for wave simulation in a partially saturated rock, including capillarity pressure effects. A second slow wave due to these effects has been observed for the first time. (Capillarity effects are not included in Biot's classical theory.) The differential equations are based on a three-phase Biot-type theory, and include viscoelastic effects to describe realistic wave attenuation. At seismic frequencies, the slow waves are quasi-static and the governing equations stiff. The latter are partitioned in a non-stiff part and a stiff part, which are solved by a standard explicit time-integration algorithm and analytically, respectively. The resulting algorithm is second-order accurate in time and has spectral accuracy in the space variable. The algorithm, which allows general material variability, provides snapshots and time histories of the different phases (particle velocities and stress components). In our simulations, the second slow mode is the faster of the slow compressional waves, and its particle motion is such that the solid and the non-wetting fluid are in phase. Future research involves the study of the conditions for which this wave can be detected in laboratory experiments. Our simulations indicate that for a clean (clay-free) partially saturated natural sandstone, subjected to a pore pressure of 30 MPa, the second slow wave (labeled P3) is a propagating mode with a velocity of 300 m/s.

Appendix A. Phase velocity and attenuation factor

Following Santos et al. [26], the phase velocity of compressional waves is (e.g. [6]),

$$v_{\rm p} = \left[{\rm Re}\left(\frac{1}{v_{\rm c}} \right) \right]^{-1}, \tag{A.1}$$

where $v_{\rm c}$ is the complex velocity satisfying the eigenvalue equation

$$\mathbf{M}\mathbf{q} = v_{\rm c}^2(\mathbf{D} - {\rm i}\mathbf{L})\mathbf{q} \tag{A.2}$$

with $\mathbf{q}$ the eigenvectors, $\mathbf{D}$ the density matrix defined in Eq. (21),

$$\mathbf{M} = \begin{pmatrix} K_{\rm c} & B_1 & B_2 \\ B_1 & M_1 & M_3 \\ B_2 & M_3 & M_2 \end{pmatrix},$$

the stiffness matrix, and

$$\mathbf{L} = \frac{1}{\omega}{\rm diag}(0, b_{\rm n}, b_{\rm w})$$

the friction matrix. The shear phase velocity has the form (A.1), where

$$v_{\rm c} = \sqrt{N}\left[\rho - \frac{\rho_{\rm n} S_{\rm n}(g_2^* \rho_{\rm n} S_{\rm n} - g_3 \rho_{\rm w} S_{\rm w}) + \rho_{\rm w} S_{\rm w}(g_1^* \rho_{\rm w} S_{\rm w} - g_3 \rho_{\rm n} S_{\rm n})}{g_1^* g_2^* - g_3^2} \right]$$

and

$$g_1^* = g_1 - \frac{{\rm i}b_{\rm n}}{\omega} \quad \text{and} \quad g_3^* = g_3 - \frac{{\rm i}b_{\rm w}}{\omega}.$$

At low frequencies (i.e., the seismic case) the compressional and shear velocities are

$$v_{\rm p}({\rm P1}) = \sqrt{\frac{K_{\rm c} + N}{\rho}} \quad \text{and} \quad v_{\rm p}({\rm S}) = \sqrt{\frac{N}{\rho}}. \tag{A.3}$$

The attenuation factor is given by [6],

$$\alpha = -\omega\, {\rm Im}\left(\frac{1}{v_{\rm c}} \right). \tag{A.4}$$

References

[1] B. Arntsen, J.M. Carcione, Numerical simulation of the Biot slow wave in water-saturated Nivelsteiner sandstone, Geophysics 66 (2001) 890–896.
[2] J.G. Berryman, Confirmation of Biot's theory, Appl. Phys. Lett. 37 (1980) 382–384.
[3] M.A. Biot, Mechanics of deformation and acoustic propagation in porous media, J. Appl. Phys. 33 (1962) 1482–1498.
[4] T. Bourbié, O. Coussy, B. Zinszner, Acoustics of porous media, Éditions Technip, 1987.
[5] J.M. Carcione, Constitutive model and wave equations for linear, viscoelastic, anisotropic media, Geophysics 60 (1995) 537–548.
[6] J.M. Carcione, Wave fields in real media: wave propagation in anisotropic, anelastic and porous media, in: Handbook of Geophysical Exploration, vol. 31, Pergamon Press, Oxford, 2001.
[7] J.M. Carcione, Wave propagation in anisotropic, saturated porous media: plane wave theory and numerical simulation, J. Acoust. Soc. Am. 99 (5) (1996) 2655–2666.
[8] J.M. Carcione, G. Seriani, Wave simulation in frozen sediments, J. Comput. Phys. 170 (2001) 1–20.
[9] J.M. Carcione, G. Quiroga-Goode, Some aspects of the physics and numerical modeling of Biot compressional waves, J. Comput. Acoust. 3 (1996) 261–280.
[10] R.C.Y. Chin, J.G. Berryman, G.W. Hedstrom, Generalized ray expansion for pulse propagation and attenuation in fluid-saturated porous media, Wave Motion 7 (1985) 43–65.
[11] B. Fornberg, A Practical Guide to Pseudospectral Methods, Cambridge University Press, Cambridge, 1996.

[12] F. Gassmann, Uber die elastizität poröser medien, Vierteljahrsschrift der Naturforschenden 96 (1951) 1–23.
[13] A.R. Gourlay, Splitting methods for time dependent partial differential equations, in: D. Jacobs (Ed.), The State of the Art in Numerical Analysis, Academic Press, New York, 1977, p. 757.
[14] B. Gurevich, O. Kelder, D.M.J. Smeulders, Validation of the slow compressional wave in porous media: comparison of experiments and numerical simulations, Transport in Porous Media 36 (1999) 149–160.
[15] M.K. Jain, Numerical Solutions of Partial Differential Equations, Wiley Eastern, New Delhi, 1984.
[16] S.M. Jones, T.R. Astin, C. McCann, The effect of degree of saturation on ultrasonic velocity and attenuation in sandstones, in: Proceedings of the SEG Annual Meeting, Expanded Abstracts, 1997, pp. 1023–1026.
[17] O. Kelder, D. Smeulders, Observation of the Biot slow wave in water-saturated Nivelsteiner sandstone, Geophysics 62 (1997) 1794–1796.
[18] R. Kosloff, D. Kosloff, Absorbing boundaries for wave propagation problems, J. Comput. Phys. 63 (1986) 363–376.
[19] G. Mavko, T. Mukerji, J. Dvorkin, The Rock Physics Handbook: Tools for Seismic Analysis in Porous Media, Cambridge University Press, Cambridge, 1998.
[20] S. Mochizuki, Attenuation in partially saturated rocks, J. Geophys. Res. 87 (1982) 8598–8604.
[21] W.F. Murphy, K.W. Winkler, R.L. Kleinberg, Acoustic relaxation in sedimentary rocks: dependence on grain contacts and fluid saturation, Geophysics 51 (1986) 757–766.
[22] W.L. Pilant, Elastic Waves in the Earth, Elsevier, Amsterdam, 1979.
[23] T. Plona, Observation of a second bulk compressional wave in a porous medium at ultrasonic frequencies, Appl. Phys. Lett. 36 (1980) 259–261.
[24] E.J. Putzer, Avoiding the Jordan canonical form in the discussion of linear systems with constant coefficients, Am. Math. Month. 73 (1966) 2.
[25] J.E. Santos, J. Douglas Jr., J.M. Corberó, O.M. Lovera, A model for wave propagation in a porous medium saturated by a two-phase fluid, J. Acoust. Soc. Am. 87 (1990) 1439–1448.
[26] J.E. Santos, J. Douglas Jr., J. Corberó, Static and dynamic behaviour of a porous solid saturated by a two-phase fluid, J. Acoust. Soc. Am. 87 (1990) 1428–1438.
[27] C.L. Ravazzoli, J.E. Santos, J.M. Carcione, Acoustic and mechanical response of reservoir rocks under variable saturation and effective pressure, J. Acoust. Soc. Am. 113 (4), 1801–1811.
[28] R.D. Stoll, G.M. Bryan, Wave attenuation in saturated sediments, J. Acoust. Soc. Am. 47 (2) (1970) 1440–1447.
[29] G. Tao, M.S. King, M. Nabi-Bidhendi, Ultrasonic wave propagation in dry and brine-saturated sandstones as a function of effective stress: laboratory measurements and modeling, Geophys. Prospect. 43 (1995) 299–327.
[30] C.B. Vreugdenhil, Accuracy of product-formula algorithms, J. Comput. Phys. 97 (1991) 337.
[31] K. Winkler, A. Nur, Pore fluids and seismic attenuation in rocks, Geophys. Res. Lett. 6 (1981) 1–4.